Received: 30 June 2022 | Revised: 27 August 2022 | Accepted: 5 September 2022

DOI: 10.1002/msd2.12053

RESEARCH ARTICLE

IJMSD International Journal of Mechanical System Dynamics Open Access WILEY

Grating-like anechoic layer for broadband underwater sound absorption

Chenlei Yu[1,2] | Mingyu Duan[1,2,3] | Wei He[1,2] | Xin Chen[4] | Fengxian Xin[1,2] | Tian J. Lu[5,6]

[1]State Key Laboratory for Strength and Vibration of Mechanical Structures, School of Aerospace Engineering, Xi'an Jiaotong University, Xi'an, China

[2]MOE Key Laboratory for Multifunctional Materials and Structures, School of Aerospace Engineering, Xi'an Jiaotong University, Xi'an, China

[3]Department of Advanced Manufacturing and Robotics, College of Engineering, Peking University, Beijing, China

[4]Xi'an Modern Chemistry Research Institute, Xi'an, China

[5]State Key Laboratory for Mechanics and Control of Mechanical Structures, College of Aerospace Engineering, Nanjing University of Aeronautics and Astronautics, Nanjing, China

[6]MIIT Key Laboratory of Multifunctional Lightweight Materials and Structures, College of Aerospace Engineering, Nanjing University of Aeronautics and Astronautics, Nanjing, China

Correspondence

Fengxian Xin, State Key Laboratory for Strength and Vibration of Mechanical Structures, Xi'an Jiaotong University, 710049 Xi'an, China.
Email: fengxian.xin@gmail.com

Tian J. Lu, State Key Laboratory for Mechanics and Control of Mechanical Structures, Nanjing University of Aeronautics and Astronautics, 210016 Nanjing, China.
Email: tjlu@nuaa.edu.cn

Funding information

National Natural Science Foundation of China, Grant/Award Numbers: 11972185, 12032010

Abstract

To address the challenging task of effective sound absorption in the low and broad frequency band for underwater structures, we propose a novel grating-like anechoic layer by filling rubber blocks and an air backing layer into metallic grating. The metallic gratings are incorporated into the anechoic layer as a skeleton for enhanced viscoelastic dissipation by promoting shear deformation between rubber and metal plates. The introduction of an air backing layer releases the bottom constraint of the rubber, thus intensifying its deformation under acoustic excitation. Based on the homogenization method and the transfer matrix method, a theoretical model is developed to evaluate the sound absorption performance of the proposed anechoic layer, which is validated against finite element simulation results. It is demonstrated that a sound absorption coefficient of the grating-like anechoic layer of 0.8 can be achieved in the frequency range of 1294–10 000 Hz. Given the importance of sound absorption at varying frequencies, the weighted average method is subsequently used to comprehensively evaluate the performance of the anechoic layer. Then, with structural density taken into consideration, an integrated index is proposed to further evaluate the acoustic properties of the proposed anechoic layer. Finally, the backing conditions and the boundary conditions of finite-size structures are discussed. The results provide helpful theoretical guidance for designing novel acoustic metamaterials with broadband low-frequency underwater sound absorption.

KEYWORDS

underwater sound absorption, broadband, transfer matrix method, rubber coating

1 | INTRODUCTION

As an effective medium for long-distance transmission of underwater information, sound waves have been widely used in underwater reconnaissance. As a typical antireconnaissance method, a well-designed anechoic layer works to minimize the intensity of reflected sound waves by absorbing a large portion of the incident sound energy.[1] Viscoelastic materials, such as rubber and polyurethane, are often used as the matrix of the anechoic layer, because their acoustic impedance matches that of water.[2–6] When excited by incident sound waves, the polymer chains inside a viscoelastic material vibrate, which enables intramolecular frictions to consume part of the sound energy. At present, sonar technology has the characteristics of a low detection frequency with a wide band, and it is constantly expanding to low frequency. However, due to the inherently weak dissipation of typical viscoelastic materials within the low-frequency range,[7,8] the absorption of low-frequency sound remains a great challenge. Coupled with the long wavelength of low-frequency sound waves in water, it appears that, at present, the only way to effectively attenuate the sound using a traditional uniform viscoelastic material is to increase its thickness.

To improve the viscoelastic dissipation performance of rubber at low frequencies, while a variety of sound-absorbing structures have been proposed, the more mature one is the cavity resonance structure[9-14] that shows cavity-related absorption peaks at low frequencies. The cavity weakens the stiffness of rubber and reduces the natural frequency of the structure. When the frequency of incident sound is close to this natural frequency, the vibration of polymer chains in rubber is intensified, resulting in significantly increased energy dissipation via intramolecular frictions. In recent years, by periodically arranging metallic spheres or cylinders coated with soft materials in a host polymer matrix, locally resonant anechoic layers have been widely investigated.[15-21] When the frequency of a sound wave approaches the natural frequency of local resonators, the latter force the polymer chains to vibrate violently, thus achieving strong sound absorption.[16] In recent years, the development of metamaterials/metasurfaces has led to new vitality to the design of underwater anechoic layers. Typically, by periodically embedding air cavities in soft materials, bubble metasurfaces were invented, and relevant acoustic properties including sound scattering,[22-24] transmission,[25-29] and absorption[30-34] were extensively studied. High sound absorption was achieved thanks to Fabry–Perot resonance created due to interference between scattered waves from the voids and reflected waves from the steel backing, as well as lumped spring–mass resonance formed with the soft material and steel backing. For enhanced low-frequency sound absorption, metallic structures with different topologies were introduced into rubber to form spring–mass resonant metamaterials.[35-38] In addition, quasi-Helmholtz resonance metamaterials constructed by incorporating rubber into the Helmholtz structure were exploited for low-frequency underwater sound absorption.[39-41] Generally speaking, however, the resonant anechoic structures proposed hitherto by existing studies show a narrow frequency bandwidth of sound absorption, thus restricting their practical applications.[17,42,43] Therefore, broadening the effective absorption bandwidth of low-frequency sound waves has become the focus of underwater acoustic research.[17,42] It should be mentioned that, focusing upon underwater low-frequency broadband sound absorption structure, Qu et al.[44] reduced the equivalent longitudinal sound speed by mixing tungsten into polyurethane and realized subwavelength as well as broadband sound absorption by designing the distribution of Fabry–Perot resonance, which has practical significance.

To meet the pressing practical demands, more research is needed in the design of low-frequency broadband absorption structures. In recent years, novel lightweight hybrid structures constructed by combining two or more materials (or structures) in such a way as to achieve attributes not offered by individual constituent have received increasing attention.[45-47] Cellular lattice trusses, because of the large number of cavities inside, have been selected for such hybrid design. For instance, upon filling the interstices of aluminum corrugations with trapezoidal aluminum honeycomb blocks, the new hybrid structure showed considerable enhancement in specific strength and specific energy absorption.[48] In the field of sound absorption, Tang et al.[49-51] proposed a hybrid acoustic metamaterial by using a honeycomb-corrugation hybrid as a sandwich core and introducing perforations on both the top face sheet and corrugation. The hybrid idea confers the structure with superior broadband low-frequency sound absorption as well as excellent mechanical stiffness/strength, which confirms the potential of the hybrid idea in structural design.

Previously, inspired by the idea of hybrid design, we proposed an underwater anechoic layer filled with rubber between metal plates and demonstrated that the new structure improved the sound-absorbing performance of rubber by enlarging the shearing strain increment of rubber density as follows.[52] The underlying physical mechanisms are as follows: due to significant impedance mismatch between rubber and metal, vibration between the two is often uncoordinated under acoustic excitation; therefore, by assuming that the rubber block is well bonded to the metallic gratings, molecular chain frictions inside the viscoelastic rubber near each rubber–grating interface are considerably enhanced, thus enabling more acoustic energy to be dissipated. However, since the wavelength of a low-frequency sound wave is much larger than the thickness of the structure, storage of the energy of sound in rubber is difficult, and only its upper part vibrates at low frequencies. In other words, based on the original design of the grating-like anechoic structure (i.e., without air backing), it is difficult to convert the energy of a low-frequency sound wave into the kinetic energy of rubber. Thus, increasing the vibration of bottom rubber and converting more energy of low-frequency sound wave into the kinetic energy of rubber are the key for enhanced sound absorption performance. Therefore, in the present study, we introduce an air layer at the bottom of rubber to address this issue, as shown schematically in Figure 1A. It is anticipated that the deformability of the bottom rubber can be enhanced by releasing the fixed boundary condition via the introduced air layer, thus enabling improvement of the low-frequency absorption performance of the new anechoic layer.

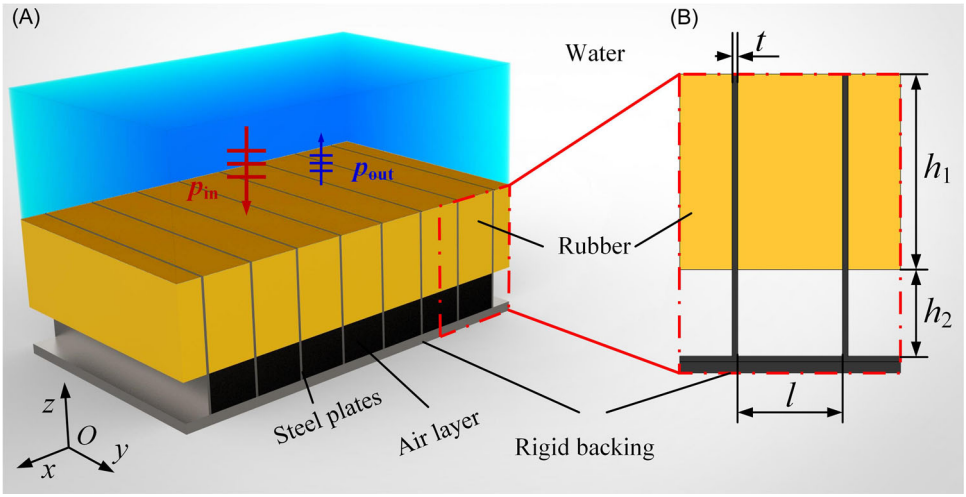

FIGURE 1 (A) Schematic of the grating-like anechoic layer and (B) two-dimensional unit cell.

The paper is organized as follows: first, a theoretical model is developed to calculate the sound absorption properties of the grating-like anechoic layer. For viscoelastic materials such as rubber, given that the complex modulus model and the complex viscosity model are equivalent, the latter is used to characterize the proposed structure. The problem is thence formulated as wave propagation in vertical slits, which enables the development of a theoretical model based on homogenization and the method of transfer matrix. Subsequently, for validation, we conducted finite element (FE) simulations. The validated model is then adopted to calculate the sound absorption coefficient in the frequency range of 1294–10 000 Hz. To explore physical mechanisms underlying the superior broadband underwater acoustic performance, vibration velocity, and viscous energy dissipation are investigated. Then, the influence of key geometric parameters is quantified, and the effects of frequency weighting and mass density of the anechoic layer on structural design are discussed. Finally, considering the actual engineering requirements, the influence of backing conditions and boundary conditions on the sound absorption performance of the structure is studied.

2 | THEORETICAL MODEL

As shown in Figure 1A, an incident plane sound wave normally impinges on the proposed anechoic layer immersed in water. The anechoic layer is periodic and composed of three main parts: rubber blocks, air layers, and the parallel steel plates connected with rigid steel backing. Each rubber block is closely bonded to adjacent steel plates, with no slip allowed at the interfaces between the steel plates and rubber. The air layer is located between the bottom of the rubber block and the steel backing. As the steel plates are periodically arranged in the x-direction and infinite in the y-direction, the grating-like anechoic layer can be evaluated via a two-dimensional (2D) unit cell; Figure 1B. The thickness of the rubber block and that of the air layer are h_1 and h_2, respectively. The thickness of a single steel plate is t and that of the plate spacing is l. Besides, the steel plates are assumed to be rigid because steel is hundreds of times stiffer than rubber.

Typically, viscoelastic material is a kind of material with both elasticity and viscosity. When viscosity is dominant, such as in petroleum, it is commonly characterized using the complex viscosity model $\mu_c = \mu(1 + j\gamma_s)$,[53] while when elasticity is dominant, such as in rubber, it is usually characterized using the complex modulus model $G_c = G(1 + j\eta_s)$,[54,55] where G_c and η_s are, respectively, the complex shear modulus and the loss factor, and μ_c and γ_s are the complex viscosity and the elastic phase, respectively. With small deformation assumed, when rubber is subjected to the excitation of a harmonic wave, the solid constitutive model using complex modulus is completely equivalent to the fluid constituting using complex viscosity and G_c and μ_c can be related by

$$\mu_c = -j \cdot \frac{G_c}{\omega}. \tag{1}$$

Equation (1) describes the conversion between the complex viscosity model and the complex modulus model.

As shown in Figure 2A, in the direction of sound wave propagation, the anechoic layer is divided into two layers. If the complex modulus model of rubber is used, the complex waveform transitions between rubber and metal plates are difficult to solve explicitly. However, upon using the complex viscosity model, the propagation of sound in the first layer can be regarded as wave propagation in fluid in parallel slits. To deal with this problem, a homogenization method is usually adopted, that is, the influence of viscosity between the grating and rubber on the vibration of rubber is transformed into a complex increment of rubber density as follows[56]:

$$\rho_{eq}^1 = \frac{\rho_r}{\phi}\left[1 - \frac{1}{Q\sqrt{j}}\tanh(Q\sqrt{j})\right]^{-1}, \tag{2}$$

$$K_{eq}^1 = \frac{\rho_r}{\phi}c_l^2(1 + j\eta_l), \tag{3}$$

where ρ_{eq}^1 and K_{eq}^1 are, respectively, the equivalent density and equivalent modulus of the first layer, ρ_r is the density of rubber, $\phi = l/(t + l)$ represents the proportion of rubber in the first layer, $j = \sqrt{-1}$ is the imaginary unit, c_l is the compressional wave speed, and η_l is the loss factor of the compression modulus, $Q = a\sqrt{\omega\rho_r/\mu_r}/2$ denotes the ratio of plate spacing a to the thickness of viscous boundary layer $\delta = \sqrt{2\mu_c/(\omega \cdot \rho_r)}$, $\omega = 2\pi f$ is the angular frequency, and f is the frequency of sound. Detailed derivations of these equations can be found in our previous study.[52] According to Equation (1), $\mu_c = -j\rho_r c_s^2(1 + j\eta_s)/\omega$, where c_s is the shear wave speed and η_s is the loss factor of the shear modulus. Then, the wavenumber and characteristic impedance of the rubber layer can be expressed, respectively, as $k_{eq}^1 = \omega\sqrt{\rho_{eq}^1/K_{eq}^1}$ and $Z_{eq}^1 = \sqrt{K_{eq}^1 \cdot \rho_{eq}^1}$.

For the second layer of air with steel backing, the plate spacing is much larger than the viscous boundary layer of air, and hence viscous dissipation is negligible compared to that of the first layer. Consequently, for theoretical calculations, the second layer can be regarded as a homogenized air layer, whose equivalent dynamical density and bulk modulus are the same as those of air: $\rho_{eq}^2 = \rho_{air}$ and $K_{eq}^2 = \rho_{air}c_{air}^2$, where ρ_{air} and c_{air} are the density and sound speed of air, respectively. Similarly, the wavenumber and characteristic impedance of the air layer are determined by $k_{eq}^2 = \omega\sqrt{\rho_{eq}^2/K_{eq}^2}$ and $Z_{eq}^2 = \sqrt{K_{eq}^2 \cdot \rho_{eq}^2}$.

Upon the above homogenization, the grating-like anechoic layer is simplified to a multilayer sound-absorbing structure, as shown in Figure 2B. When sound propagates in such an anechoic layer, the pressure and velocity of sound satisfy:

$$\begin{bmatrix} p(A) \\ v(A) \end{bmatrix} = \boldsymbol{T}\begin{bmatrix} p(B) \\ v(B) \end{bmatrix}, \tag{4}$$

where $p(A)$ and $v(A)$ represent, respectively, the sound pressure and the vibration velocity of the incident surface, while $p(B)$ and $v(B)$ represent the sound pressure and the vibration speed of the transmission surface, respectively. $\boldsymbol{T}$ is the transfer matrix of the structure, given by

$$\boldsymbol{T} = \begin{bmatrix} \cos k_{eq}^1 h_1 & jZ_{eq}^1 \sin k^1 h_1 \\ j \sin k_{eq}^1 h/Z^1 & \cos k_{eq}^1 h_1 \end{bmatrix}\begin{bmatrix} \cos k_{eq}^2 h_2 & jZ_a \sin k_{eq}^2 h_2 \\ j \sin k_{eq}^2 h_2/Z_a & \cos k_{eq}^2 h_2 \end{bmatrix}. \tag{5}$$

Equations (4) and (5) present the transfer matrices of the structure. With the back surface of the structure taken as fixed, namely, $v(B) = 0$, the surface acoustic impedance of the front surface can be obtained as

$$Z_s = \frac{p(A)}{v(A)} = \frac{T_{11}}{T_{21}}. \tag{6}$$

To evaluate the sound absorption performance of the proposed anechoic layer, the absorption coefficient α is calculated by

$$\alpha = 1 - |(z_s - 1)/(z_s + 1)|^2, \tag{7}$$

where $z_s = Z_s/Z_0$ is the relative acoustic surface impedance of the anechoic layer, $Z_0 = \rho_0 c_0$ is the characteristic impedance of water, and ρ_0 and c_0 are the density and sound speed of water, respectively.

3 | NUMERICAL MODEL

To validate the theoretical model, a 2D FE model considering acoustic–structure coupling is developed with COMSOL multiphysics,[55] as shown in Figure 3. The perfect matching layer (a domain that can absorb all incoming waves, which is added to simulate the

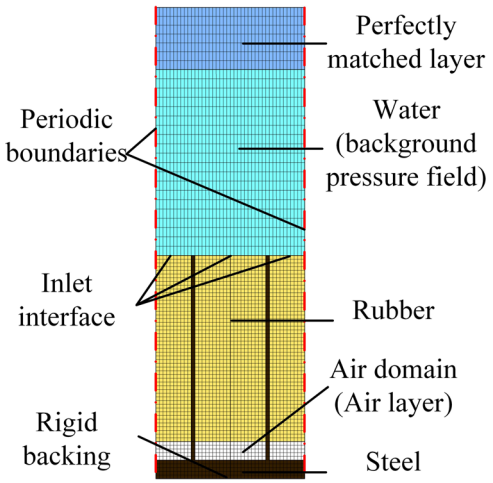

FIGURE 3 Finite element model and mesh generation

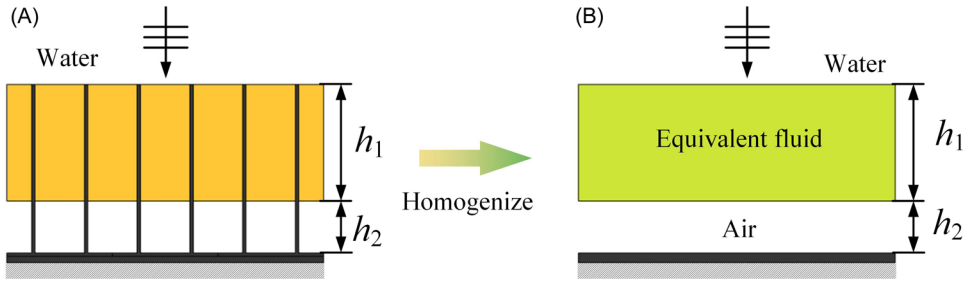

FIGURE 2 Equivalent calculation model: (A) actual configuration of the grating-like anechoic layer and (B) equivalent theoretical model

infinite acoustic domain), the background pressure field, and the air layer are modeled in the Pressure Acoustics module, while the rubber blocks and steel plates are modeled in the Solid Mechanic module. The perfectly matching layer (PML) is used to simulate the anechoic end, and the incident plane sound wave is applied to the background pressure field. As to the boundary conditions, the lateral boundaries are set as periodic boundaries, while the bottom is fixed according to the assumption of rigid backing. With the FE model, the sound absorption coefficient can be calculated as

$$\alpha = 1 - R^2 = 1 - \frac{\langle p_{re}\rangle^2}{\langle p_{in}\rangle^2}, \tag{8}$$

where p_{in} and p_{re} are the incident and reflected sound pressure, respectively, and $\langle\cdot\rangle$ represents the surface average over the inlet interface.

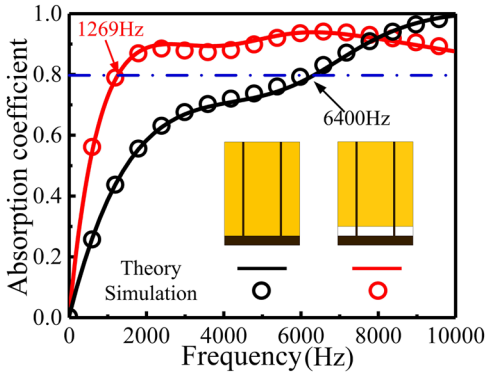

FIGURE 4 Theoretically predicted and numerically calculated sound absorption coefficients for a grating-like anechoic layer with and without an air backing layer, the former denoted as GALA and the latter as GAL

4 | RESULTS AND DISCUSSION

4.1 | Sound absorption performance

The relevant physical parameters of rubber are listed in Table 1, which are assumed to remain constant over the whole frequency range considered for simplicity. The density and sound speed of water are 1000 kg/m^3 and 1500 m/s, respectively, and those of air are 1.293 kg/m^3 and 340 m/s, respectively. For steel, the density is 7850 kg/m^3, Young's modulus is 209 GPa, and the Poisson ratio is 0.3. Geometric parameters of the anechoic layer are as follows: $h_1 + h_2 = 50$ mm, $l = 19$ mm, and $t = 1$ mm. In this case, the volume proportion of rubber is $\phi = 0.95$ in the rubber layer. Here, two different structures are compared, that is, $h_2 = 5$ mm for the grating-like anechoic layer with the air backing layer (GALA) and $h_2 = 0$ mm for the one without the air backing layer (GAL). It should be pointed out that the proposed method is not limited to specific geometrical dimensions considered above, and has general applicability. The influence of key geometrical parameters on sound absorption of the grating-like anechoic layer is discussed in Section 4.2.

Figure 4 compares the analytical predictions of sound absorption coefficient with FE simulation results for both GALA and GAL. Good agreement is achieved between the theoretical and numerical results, thus validating the proposed theoretical model. The results demonstrate the appreciable superiority of GALA over GAL. In the absence of air backing, the GAL has excellent high-frequency performance above 6400 Hz but an insufficient sound absorption coefficient below 6400 Hz, which limits its practical application. In contrast, with the help of air backing, the GALA enables a shift of its minimum effective absorption frequency (the first frequency when sound absorption coefficient $\alpha > 0.8$) from 6400 Hz to a much lower frequency (1269 Hz), which confirms broadband and strong sound absorption. The average absorption coefficient of the GALA is 0.86, which demonstrates a 19% enhancement in comparison with that (0.72) achieved by the GAL. Relative to GAL, it is obvious that the improvement at low frequencies is induced by the air backing layer under the rubber.

From the perspective of manufacturability, due to the simple structure of the proposed anechoic layer with air backing, two common methods can be adopted to prepare the structure: the method of pouring and curing and the method of block cutting and bonding. Although the introduction of the air layer somewhat increases the difficulty of preparation, this increase is acceptable in comparison with the significantly enhanced sound absorption performance of the anechoic layer, especially at low frequencies. It should be pointed out that the introduction of an air layer increases the deformation of the anechoic layer under hydrostatic pressure; the modulus of rubber also increases with hydrostatic pressure. As a result, increasing the hydrostatic pressure shifts the sound absorption coefficient of the GALA to higher frequencies. However, since the steel gratings introduced in the proposed structure can prevent the inserted rubber layers from deforming, it is anticipated that hydrostatic pressure would have a relatively weak effect on the absorption performance of the structure. That is to say, the present theoretical and simulation results are valid under the condition that the deformation of rubber caused by hydrostatic pressure is negligible.

To explore the physical mechanisms underlying the superior absorption performance of the proposed grating-like anechoic layer, comparisons among particle vibration velocity and viscous energy dissipation at the frequency of 2000, 6000, and 10 000 Hz in one unit cell of both GAL and GALA are performed, as shown in Figures 5A,B. The colored area shows rubber blocks inside the anechoic layers. At low frequencies (such as 2000 Hz), the vibration velocity of GALA is much greater than that of GAL, especially in the lower portion of the structure. Near the rubber–plate interfaces, the shear deformation of GALA is considerably intensified than that of GAL, thus dissipating more acoustic

TABLE 1 Physical parameters of rubber

Material parameter	ρ_r	c_l	η_l	c_s	η_s
Value	900 kg/m^3	1000 m/s	0.3	100 m/s	0.9

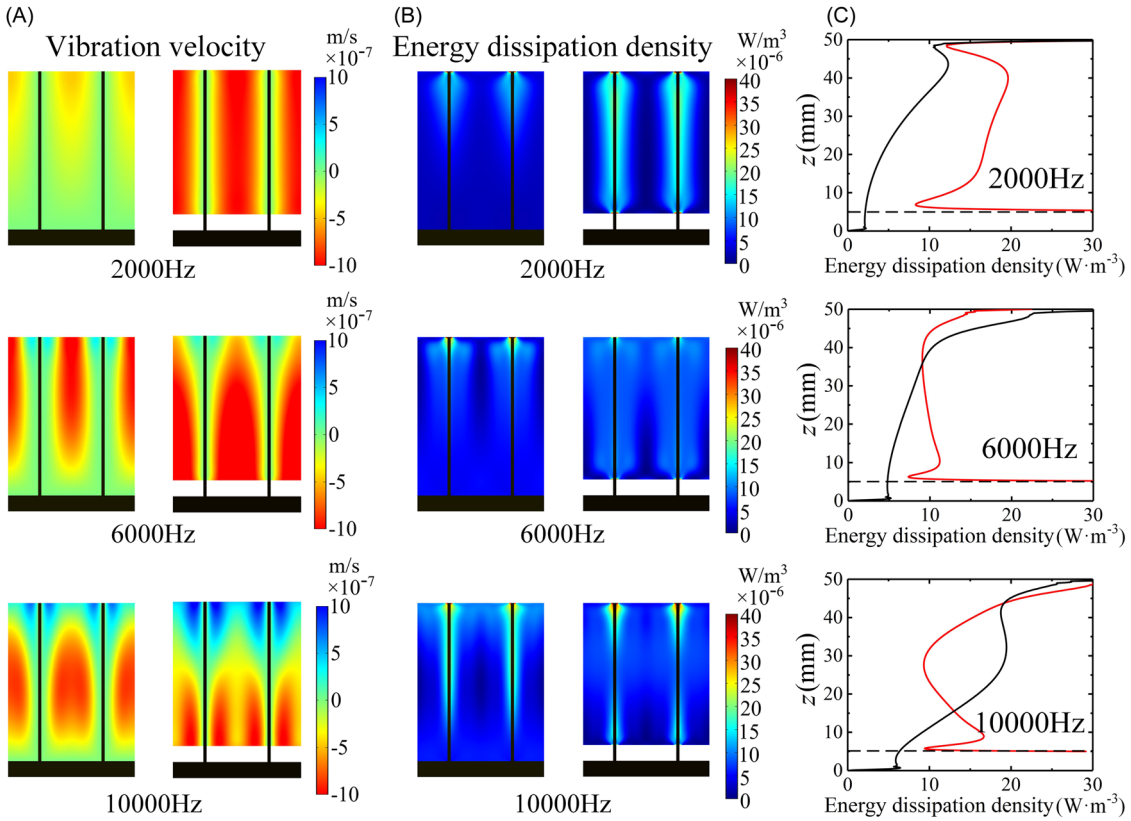

FIGURE 5 (A) Comparison of vibration velocity distributions between GAL and GALA, (B) comparison between distributions of energy dissipation density in GAL and GALA, and (C) comparison of distributions of energy dissipation density along the rubber–plate interface in GAL and GALA, all plotted at selected frequencies of 2000, 6000, and 10 000 Hz

energy. This is mainly attributed to increased rubber deformation caused by the introduction of air backing layer. For a more quantitative evaluation, the distribution of energy dissipation density on the rubber–plate interface is presented in Figure 5C. Compared with GAL, although the amount of rubber in GALA is less, the viscous energy dissipation is more than twice that of GAL. In the intermediate- and high-frequency bands (i.e., 6000 and 10 000 Hz), the two structures show similar particle vibration velocities, and viscous energy dissipation remains concentrated near rubber–plate interfaces. The results presented in Figure 4 for GAL (i.e., without air backing) and GALA (i.e., with air backing) reveal that the fundamental reason for the poor low-frequency sound absorption of the former is its weak ability to store low-frequency sound energy. The introduction of an air layer as the backing of rubber perfectly solves this problem. As can be seen in Figure 5A, the air layer releases the fixed boundary condition of rubber, thus providing more space for the rubber to vibrate. Further, in sharp contrast to the original design (GAL), the new design (GALA) not only enables the lower portion of rubber to vibrate and hence store sonic energy but also enhances the vibration of the upper portion of rubber. Eventually, the kinetic energy of rubber is converted into heat due to viscous dissipation at rubber–metal interfaces. Therefore, the introduced air layer can significantly improve the acoustic performance of rubber-filled gratings.

From another point of view, the sound absorption capacity of the proposed anechoic layer is mainly determined by two factors: the ability to convert acoustic energy into kinetic energy, that is, the acoustic resistance $\mathrm{Im}(Z_s)$, and the ability to convert kinetic energy into heat, that is, the acoustic reactance $\mathrm{Re}(Z_s)$. To achieve good sound absorption, $\mathrm{Im}(Z_s) \to 0$ and $\mathrm{Re}(Z_s) \to 1$ need to be satisfied simultaneously, which means that as much incident sound energy as possible can be converted into kinetic energy and then dissipated by the anechoic layer. From the comparison of acoustic resistance between GAL and GALA in Figure 6A, it is clear that the acoustic resistance is not sensitive to the air layer below 2000 Hz, which means that the embedded air layer does not affect the kinetic energy dissipation capacity of the anechoic layer at low frequencies. Besides, the acoustic reactance is considerably improved at low frequencies due to the introduction of an air layer, as shown in Figure 6B. Together with the sound absorption coefficient of Figure 4, these noticeable features of resistance and reactance indicate that the air layer can effectively improve the low-frequency energy conversion capability of the anechoic layer, thereby improving its sound absorption performance.

4.2 | Parametric study

To explore the influence of key geometrical parameters on the sound absorption performance of a grating-like anechoic layer, the sound absorption spectrum as a function of upper rubber layer

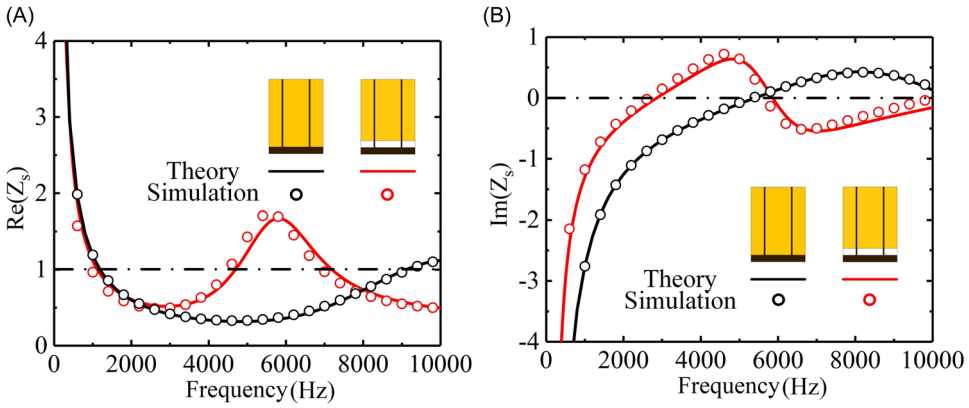

FIGURE 6 (A) Real part and (B) imaginary part of normalized surface impedance of GAL and GALA, represented separately by black and red curves, respectively

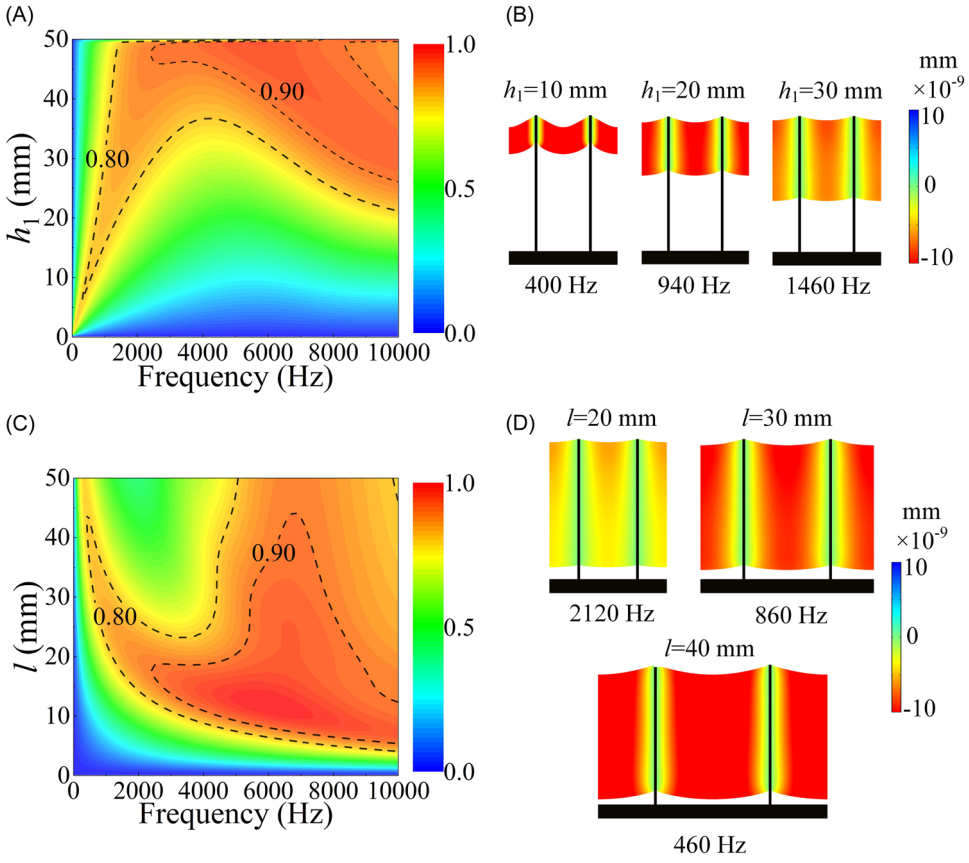

FIGURE 7 (A) Effect of air-layer thickness h_1 on the sound absorption coefficient, with l = 19 mm. (B) Displacement of the anechoic layer at absorption peak frequencies (400 Hz for h_1 = 10 mm, 940 Hz for h_1 = 20 mm, and 1460 Hz for h_1 = 30 mm), with l = 19 mm. (C) Effect of plate spacing l on the sound absorption coefficient, with h_1 = 45 mm and h_2 = 5 mm. (D) Displacement of the anechoic layer at absorption peak frequencies (2120 Hz for l = 20 mm, 860 Hz for l = 30 mm, and 460 Hz for l = 40 mm), with h_1 = 45 mm and h_2 = 5 mm

thickness h_1 and plate spacing l is calculated using the theoretical model, as shown in Figure 3, with the total thickness of the anechoic layer fixed at $h_1 + h_2$ = 50 mm. In Figure 7A, while the thickness of rubber h_1 is varied, the plate spacing is set to l = 19 mm. Decreasing h_1 leads to a reduction in the absorption coefficient within the mid- and high-frequency range. Interestingly, an absorption peak is present in the spectrum at low frequencies, which shifts to ever lower frequencies as h_1 is reduced. The physical mechanism underlying this phenomenon is the resonance of the rubber–grating system, similar to a cantilever beam fixed at both ends. To demonstrate this, for selected values of h_1, the displacement of the anechoic layer at the frequency corresponding to its

absorption peak is shown in Figure 7B. When the frequency of sound is close to the resonant frequency, the rubber oscillates violently, thus forming a narrow sound absorption band. When the rubber layer becomes thinner, the stiffness of the system decreases, moving the resonance to lower frequencies.

With h_1 = 45 mm and h_2 = 5 mm, the effect of plate spacing l on the sound absorption spectrum is shown in Figure 7C. When the plate spacing is increased, it is not surprising to find an absorption peak at low frequencies, which can be explained by the resonance of the system consisting of rubber and steel grating. As the plate spacing increases, the stiffness of the system formed by the rubber layer and vertical plates decreases, the resonance frequency shifts to low frequencies, the bandwidth of the absorption peak narrows, and the magnitude of the peak becomes smaller, as shown in Figure 7D.

5 | COMPREHENSIVE SOUND ABSORPTION PERFORMANCE

5.1 | Weighted average sound absorption coefficient

In this section, the weighted average sound absorption coefficient $\bar{\alpha}$ in the frequency range of 0–10 000 Hz is used to evaluate the sound absorption performance of the proposed anechoic layer. By using the developed theoretical model, $\bar{\alpha}$ is calculated as

$$\bar{\alpha} = \frac{\sum_0^{10000} \alpha W}{\sum_0^{10000} W}, \tag{9}$$

where $W = W(x)$ is the weight function at different frequencies, which can be adjusted according to specific requirements. In the current study, two cases are chosen: $W(x) = 1$, $1 \le f \le 10000$ for average in the frequency range of 0–10 000 Hz, and the case of average in the frequency range of 500–2000 Hz as $W(x) = 0$ for $f < 500$, $W(x) = 1$ for $500 \le f \le 2500$, and $W(x) = 0$ for $f > 2500$.

The average sound absorption within the frequency band is mapped on the spectrum of air-layer thickness h_1 and plate spacing l, as shown in Figures 8A,B. For the broadband case (i.e., 0–10 000 Hz), the range of structural parameters corresponding to an average sound absorption coefficient greater than 0.8 is focused on $h_1 > 25$ mm and $10 < l < 30$ mm. By contrast, for the low-frequency case (i.e., 500–2000 Hz), the range of structural parameters corresponding to an average sound absorption coefficient greater than 0.8 is focused on $h_1 > 25$ mm and $18 < l < 28$ mm. It can be seen that the grating-like anechoic layer is flexible to meet different frequency and frequency band sound absorption requirements.

5.2 | Optimization

To obtain the maximum weighted average absorption coefficient, the anechoic layer is optimized within the key parameter space of (h_1, l). Upon fixing its total thickness as $h_1 + h_2$ = 50 mm, the optimization problem can be described as

$$\begin{aligned} \max \quad & \bar{\alpha} \\ s.t. \quad & h_1 + h_2 = 50 \text{ mm}, \\ & 0 \le h_1 \le 50 \text{ mm}, \\ & l > 0 \text{ mm}. \end{aligned} \tag{10}$$

This optimization problem is solved using the genetic algorithm (GA) that is often used to find the approximate global optimal solution of a specific function in a large search space. The optimization results are (h_1 = 49 mm, l = 18 mm) for the case of 0–10 000 Hz and (h_1 = 48 mm, l = 26 mm) for the case of 500–2000 Hz.

Figure 9 presents the optimized sound absorption coefficients. For the broadband case, the sound absorption coefficient reaches 0.859, but the low-frequency sound absorption performance is relatively weak. In contrast, for the low-frequency case, the sound absorption coefficient is optimized to perform much better in the frequency range of 500–2000 Hz, achieving an average absorption coefficient of 0.824 in this frequency band. The results show that the proposed anechoic layer has great advantages in broadband sound absorption.

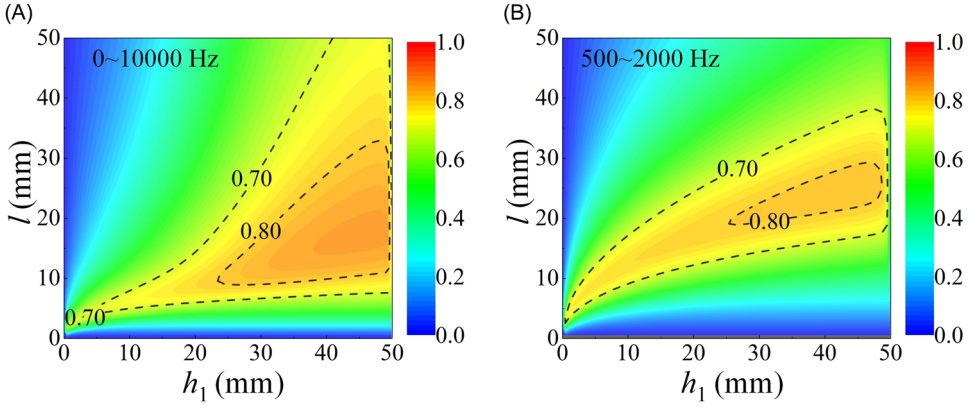

FIGURE 8 Effects of rubber thickness h_1 and plate spacing l on the average sound absorption coefficient in the frequency range of (A) 500–2000 Hz and (B) 0–10 000 Hz

5.3 | Lightweight evaluation

In practice, as an additional functional structure, the proposed anechoic layer inevitably increases the weight of a submarine and reduces its flexibility. Therefore, it is necessary to evaluate the lightweight design of the anechoic layer. As a preliminary study, an integrated performance index accounting for both (weighted average) sound absorption coefficient and mass density is introduced as follows

$$\gamma = \frac{\bar{\alpha}}{\bar{\rho}}, \tag{11}$$

where $\bar{\rho}$ is the normalized mass density, defined as the ratio of the mass density of the anechoic layer to the density of water, and is defined as

$$\bar{\rho} = \frac{\rho_{Fe}(h_1 + h_2)t + \rho_r h_1 a + \rho_a h_2 a}{(h_1 + h_2)(a + t)\rho_0}. \tag{12}$$

For illustration, let the total thickness of the anechoic layer and the thickness of steel plates be fixed at $h_1 + h_2 = 50$ mm and $t = 1$ mm, respectively. Figure 10 plots the integrated performance index γ in the frequency range of 0–10 000 Hz as a function of rubber layer thickness

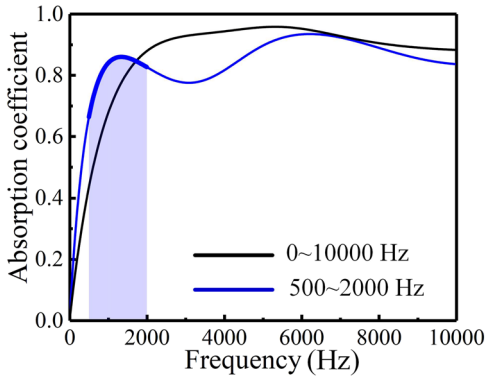

FIGURE 9 Sound absorption coefficient of an anechoic layer with optimized structural parameters

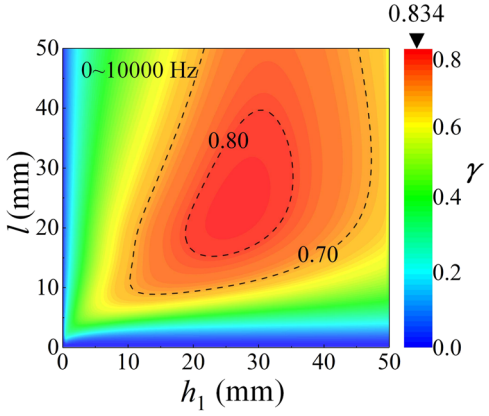

FIGURE 10 Integrated performance index considering both the sound absorption coefficient and the mass density of an anechoic layer

h_1 and plate spacing l. The feature of the points having the same color is that the structures designed with the coordinates of these points have the same γ. The results demonstrate that an anechoic layer constructed with a thick rubber layer and narrow plate spacing or a thin rubber layer and long plate spacing has inferior performance. In addition, the maximum γ exists in the region around the parameter point ($h_1 = 25$ mm, $l = 25$ mm), which means that the best sound absorption with the least structure mass is achieved in this configuration.

5.4 | Evaluation of backing effects

The anechoic layer attached to an underwater vehicle actually works under complex backing conditions. Thus, the effects of backing on the present grating-like anechoic layer should be considered for actual applications.[18,38,57] To this end, we investigated the sound absorption performance of the GALA with a backing of a 10-mm-thick steel plate[58] under three common backing conditions: rigid backing, water backing (followed by half-infinite water), and air backing (followed by half-infinite air). The thicknesses of the anechoic layer and the air layer were fixed at 50 and 5 mm, respectively. Based on the FE model detailed in Section 1, we developed FE models with two-sided infinite fluid domains for water and air backing samples, as shown schematically in the insets of Figure 11A. For each FE model, the sound absorption coefficient is calculated using $\alpha = 1 - R^2 - T^2$, where $T = p_{tr}/p_{in}$ is the transmitted sound pressure coefficient and p_{tr} is the transmitted sound pressure.

Figure 11A compares the sound absorption coefficients obtained numerically for the three backing cases. It can be seen that, for the cases considered, the backing effect is mainly manifested in the relatively low-frequency range. The sound absorption coefficient of the GALA with water backing is consistently lower than that with rigid backing, with a shift to higher frequencies. This is because the acoustic impedance of water is close to that of steel, so that the transmission of low-frequency sound waves increases, as shown in Figure 11B. For the air backing case, the anechoic layer and the backing steel plate form a mass–spring resonant system to improve the relative motion between rubber and steel gratings, as shown in the displacement distribution of Figure 11B. Therefore, the energy dissipation caused by the resonance leads to a new absorption peak at 2000 Hz (Figure 11A). Nonetheless, at frequencies below 1100 Hz, the results of Figure 11A demonstrate that the performance with air backing is inferior to that with rigid backing. This is because air and water backings are both weak constraints, and hence the rubber and steel gratings essentially move in the same direction at sufficiently low acoustic frequencies: the relative movement between the rubber and metal grille is thus weakened, causing inferior absorption performance.

5.5 | Evaluation of boundary conditions

The above study is based on wave propagation in an infinite periodic 2D medium. However, in practice, the rubber layer as well as the

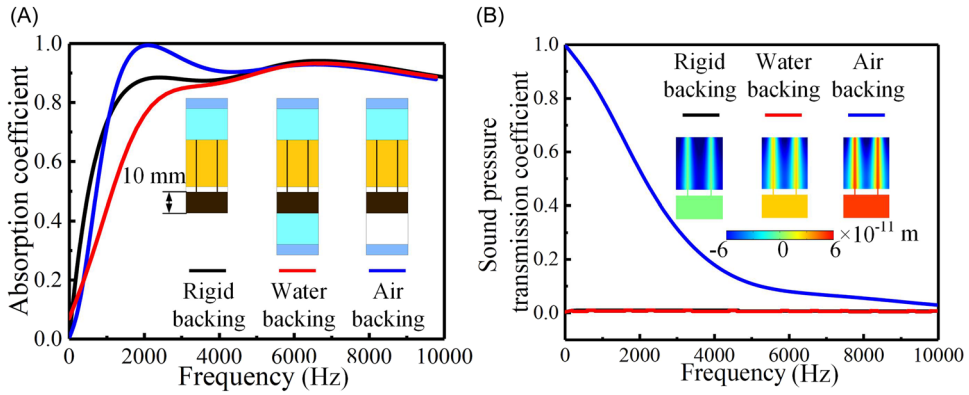

FIGURE 11 Effects of backing on the underwater acoustic property of GALA. (A) Schematics and sound absorption coefficients of GALA with rigid backing, water backing, and air backing. (B) Sound pressure transmission coefficients and spatial distribution of displacement inside GALA with different backing conditions at 2000 Hz

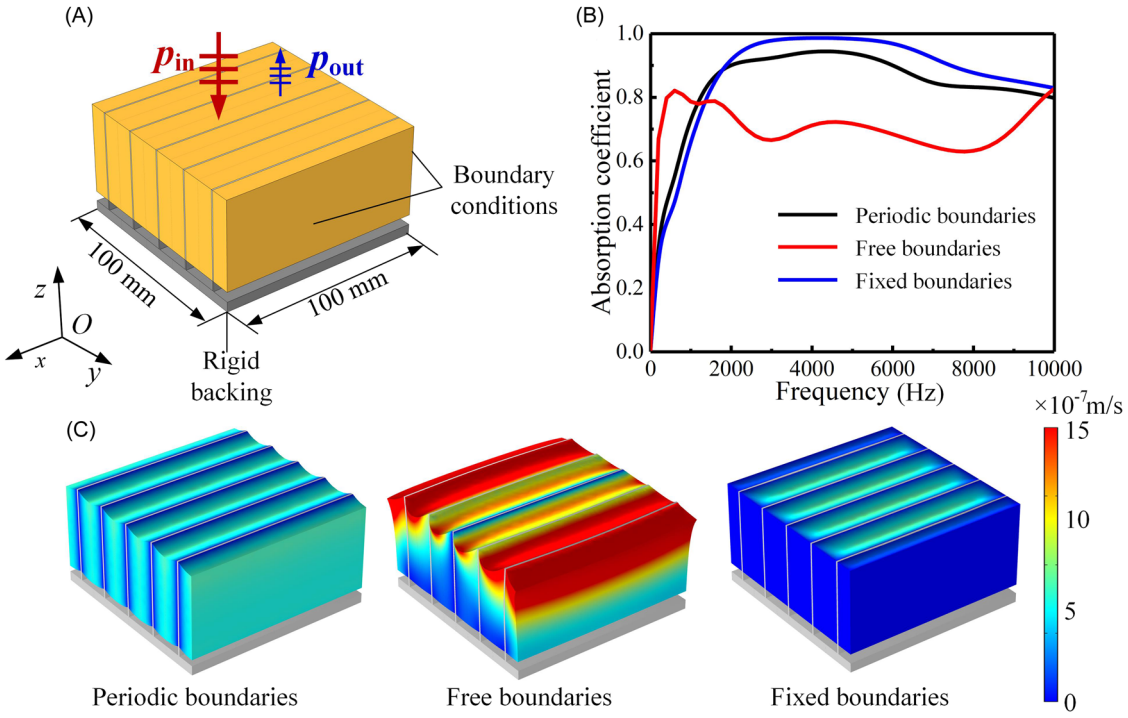

FIGURE 12 Boundary effects on acoustic performance of finite-sized GALA, with a periodic boundary, a free boundary, and a fixed boundary considered. (A) Schematic of GALA with a finite size. (B) Sound absorption coefficients of GALA with different boundary conditions. (C) Vibration velocity distribution of GALA with different boundary conditions at 800 Hz

steel plates have finite sizes and are associated with different boundary conditions. To explore the effects of boundary on the underwater sound absorption performance of grating-like anechoic layers, we developed a three-dimensional (3D) FE model with a *x*–*y* cross-sectional area of 100 mm × 100 mm, as shown in Figure 12A. The thicknesses of the anechoic layer and the air layer were fixed at 50 and 5 mm, respectively. On this basis, we obtained numerical results of the sound absorption coefficient for GALA with a periodic boundary, a free boundary, and a fixed boundary, as shown in Figure 12B. At frequencies below 1000 Hz, the free boundary sample performs better than the periodic-boundary sample, because the release of surrounding constraints of the free-boundary sample enables a larger vibration of rubber at low frequencies. For intuitive understanding, the results of Figure 12C illustrate how the boundary condition affects the vibration velocity of GALA at 800 Hz, with the red area indicating the highest vibration speed. However, it should be noted that the velocity of rubber in the free boundary sample has components in the *x* and *y* directions due to the lack of constraints, enabling the steel plate to vibrate synchronously with the rubber around it. As a result, shear deformation at the interface is decreased,

resulting in weak sound absorption performance within the full frequency band. As for the rigid boundary sample, the reinforcement of surrounding constraints increases the rigidity of the system composed of rubber and metal grating, causing the sound absorption curve to slightly shift toward higher frequencies. In addition, the fixed boundaries at both ends of the grid slits increase the surfaces available to constrain the rubber layer, leading to enhanced viscous dissipation. Thus, the sound absorption performance is superior to the case of the periodic boundary.

6 | CONCLUSIONS

A novel grating-like anechoic layer with superior broadband sound absorption has been proposed by filling rubber blocks into metallic grating connected with a rigid metallic backing, followed by the addition of an air layer to separate the rubber block and metallic backing. To predict the sound absorption performance of the anechoic layer, a theoretical model is established by applying the homogenization method and the transfer matrix method. Numerical simulations with the method of FEs are performed to validate the theoretical model, with good agreement achieved between the theoretical and numerical results. The proposed method based on a complex viscosity model is actually not limited to the above special structure and has general applicability for rubber–metal hybrid structures.

It is demonstrated that the additional air layer under the rubber block improves low-frequency sound absorption by enhancing the ability of low-frequency energy conversion from sound into kinetic energy of the anechoic layer. Upon reducing the rubber layer thickness or increasing the plate spacing, an absorption peak greater than 0.8 appears at low frequency, depending on the resonance of the rubber layer. However, when the rubber layer thickness is reduced, due to insufficient high-frequency energy dissipation, high-frequency sound absorption becomes inferior, making it difficult to achieve broadband sound absorption. In contrast, increasing the plate spacing can achieve both low-frequency and broadband absorption. For weight-sensitive applications, an integrated performance index combining the average sound absorption coefficient and the average mass density of the structure is proposed. For different backing and boundary conditions, the proposed grating-like anechoic layer still maintains excellent sound absorption performance, thus providing valuable guidance for designing novel broadband underwater anechoic layers. A future study will address challenges on applying the proposed structure in underwater environments, with particular focus on the effect of hydrostatic pressure and the influence of air backing on manufacturability.

ACKNOWLEDGMENTS

This study was supported by the National Natural Science Foundation of China (11972185 and 12032010) and the Fund of Prospective Layout of Scientific Research for Nanjing University of Aeronautics and Astronautics (NUAA).

CONFLICT OF INTEREST

The authors declare no conflict of interest.

DATA AVAILABILITY STATEMENT

The data that support the findings of this study are available from the corresponding authors upon reasonable request.

ORCID

Mingyu Duan https://orcid.org/0000-0002-8413-6751
Tian J. Lu https://orcid.org/0000-0001-7795-7511

REFERENCES

1. Ivansson SM. Sound absorption by viscoelastic coatings with periodically distributed cavities. *J Acoust Soc Am*. 2006;119(6):3558-3567.
2. Sun W, Yan X, Zhu X. Dynamic mechanical and underwater acoustic properties of the polyurethane/epoxy resin blend elastomers filled with macroporous poly(vinyl acetate-co-triallyl isocyanurate) resin beads. *J Appl Polym Sci*. 2011;122(4):2359-2367.
3. Jayakumari VG, Shamsudeen RK, Rajeswari R, Mukundan T. Viscoelastic and acoustic characterization of polyurethane-based acoustic absorber panels for under water applications. *J Appl Polym Sci*. 2019;136(10):1-9.
4. Li Z, Shen Y, Zheng C, Gu X, Li J, Gao Y. Preparation and properties of fluorosilicone polyether polyurethane underwater acoustically transparent encapsulant. *Mater Today Commun*. 2019;19:402-406.
5. Cao R, Deng L, Feng Z, Zhao X, Li X, Zhang L. Preparation of natural bio-based *Eucommia ulmoides* gum/styrene-butadiene rubber composites and the evaluation of their damping and sound absorption properties. *Polymer*. 2021;213:123292.
6. Fu Y, Fischer J, Pan K, Yeoh GH, Peng Z. Underwater sound absorption properties of polydimethylsiloxane/carbon nanotube composites with steel plate backing. *Appl Acoust*. 2021;171:107668.
7. Zhong J, Zhao H, Yang H, Wang Y, Yin J, Wen J. Theoretical requirements and inverse design for broadband perfect absorption of low-frequency waterborne sound by ultrathin metasurface. *Sci Rep*. 2019;9:1.
8. Yang M, Ma G, Yang Z, Sheng P. Subwavelength perfect acoustic absorption in membrane-type metamaterials: a geometric perspective. *EPJ Appl Metamater*. 2016;2:10.
9. Fu X, Jin Z, Yin Y, Liu B. Sound absorption of a rib-stiffened plate covered by anechoic coatings. *J Acoust Soc Am*. 2015;137(3):1551-1556.
10. Ye C, Liu X, Xin F, Lu TJ. Influence of hole shape on sound absorption of underwater anechoic layers. *J Sound Vib*. 2018;426:54-74.
11. Zhong J, Zhao H, Yang H, Yin J, Wen J. On the accuracy and optimization application of an axisymmetric simplified model for underwater sound absorption of anechoic coatings. *Appl Acoust*. 2019;145:104-111.
12. Wang S, Hu B, Du Y. Sound absorption of periodically cavities with gradient changes of radii and distances between cavities in a soft elastic medium. *Appl Acoust*. 2020;170:107501.
13. Gaunaurd G. Comments on 'absorption mechanisms for waterborne sound in Alberich anechoic layers'. *Ultrasonics*. 1985;23(2):90-91.
14. Gaunaurd G. One-dimensional model for acoustic absorption in a viscoelastic medium containing short cylindrical cavities. *J Acoust Soc Am*. 1977;62(2):298-307.
15. Zhao H, Wen J, Yu D, Wen X. Low-frequency acoustic absorption of localized resonances: experiment and theory. *J Appl Phys*. 2010;107(2):1734.

16. Wen J, Zhao H, Lv L, Yuan B, Wang G, Wen X. Effects of locally resonant modes on underwater sound absorption in viscoelastic materials. *J Acoust Soc Am*. 2011;130(3):1201-1208.
17. Meng H, Wen J, Zhao H, Wen X. Optimization of locally resonant acoustic metamaterials on underwater sound absorption characteristics. *J Sound Vib*. 2012;331(20):4406-4416.
18. Zhao H, Wen J, Yang H, Lv L, Wen X. Backing effects on the underwater acoustic absorption of a viscoelastic slab with locally resonant scatterers. *Appl Acoust*. 2014;76:48-51.
19. Zhong H, Gu Y, Bao B, Wang Q, Wu J. 2D underwater acoustic metamaterials incorporating a combination of particle-filled polyurethane and spiral-based local resonance mechanisms. *Compos Struct*. 2019;220:1-10.
20. Zhao H, Liu Y, Wen J, Yu D, Wen X. Tri-component phononic crystals for underwater anechoic coatings. *Phys Lett A*. 2007;367(3):224-232.
21. Meng H, Wen J, Zhao H, Lv L, Wen X. Analysis of absorption performances of anechoic layers with steel plate backing. *J Acoust Soc Am*. 2012;132(1):69-75.
22. Skvortsov A, MacGillivray I, Sharma GS, Kessissoglou N. Sound scattering by a lattice of resonant inclusions in a soft medium. *Phys Rev E*. 2019;99(6):063006.
23. Sharma GS, Marsick A, Maxit L, Skvortsov A, MacGillivray I, Kessissoglou N. Acoustic radiation from a cylindrical shell with a voided soft elastic coating. *J Acoust Soc Am*. 2021;150(6):4308-4314.
24. Sharma GS, Skvortsov A, MacGillivray I, Kessissoglou N. Sound scattering by a bubble metasurface. *Phys Rev B: Condens Matter Mater Phys*. 2020;102(21):214308.
25. Leroy V, Bretagne A, Lanoy M, Tourin A. Band gaps in bubble phononic crystals. *AIP Adv*. 2016;6(12):121604.
26. Leroy V, Bretagne A, Fink M, Willaime H, Tabeling P, Tourin A. Design and characterization of bubble phononic crystals. *Appl Phys Lett*. 2009;95(17):171904.
27. Sharma GS, Skvortsov A, MacGillivray I, Kessissoglou N. Sound transmission through a periodically voided soft elastic medium submerged in water. *Wave Motion*. 2017;70:101-112.
28. Calvo DC, Thangawng AL, Layman CN, Jr., Casalini R, Othman SF. Underwater sound transmission through arrays of disk cavities in a soft elastic medium. *J Acoust Soc Am*. 2015;138(4):2537-2547.
29. Bretagne A, Tourin A, Leroy V. Enhanced and reduced transmission of acoustic waves with bubble meta-screens. *Appl Phys Lett*. 2011;99(22):221906.
30. Sharma GS, Skvortsov A, MacGillivray I, Kessissoglou N. On superscattering of sound waves by a lattice of disk-shaped cavities in a soft material. *Appl Phys Lett*. 2020;116(4):041602.
31. Skvortsov A, Sharma GS, MacGillivray I, Kessissoglou N. Sound absorption by a metasurface comprising hard spheres in a soft medium. *J Acoust Soc Am*. 2021;150(2):1448-1452.
32. Sharma GS, Skvortsov A, MacGillivray I, Kessissoglou N. Acoustic performance of gratings of cylindrical voids in a soft elastic medium with a steel backing. *J Acoust Soc Am*. 2017;141(6):4694-4704.
33. Sharma GS, Toyoda M, Skvortsov A, MacGillivray I, Kessissoglou N. Acoustic performance of a metascreen-based coating for maritime applications. *J Vib Acoust Trans ASME*. 2022;144(3):031015.
34. Hinders MK, Rhodes BA, Fang TM. Particle-loaded composites for acoustic anechoic coatings. *J Sound Vib*. 1995;185(2):219-246.
35. Sharma GS, Skvortsov A, MacGillivray I, Kessissoglou N. Acoustic performance of periodic steel cylinders embedded in a viscoelastic medium. *J Sound Vib*. 2019;443:652-665.
36. Gu Y, Zhong H, Bao B, Wang Q, Wu J. Experimental investigation of underwater locally multi-resonant metamaterials under high hydrostatic pressure for low frequency sound absorption. *Appl Acoust*. 2021;172:107605.
37. Lee D, Jang Y, Park J, Kang IS, Li J, Rho J. Underwater stealth metasurfaces composed of split-orifice-conduit hybrid resonators. *J Appl Phys*. 2021;129(10):105103.
38. Zhang Y, Cheng L. Ultra-thin and broadband low-frequency underwater acoustic meta-absorber. *Int J Mech Sci*. 2021;210:106732.
39. Duan M, Yu C, Xin F, Lu TJ. Tunable underwater acoustic metamaterials via quasi-Helmholtz resonance: from low-frequency to ultra-broadband. *Appl Phys Lett*. 2021;118(7):071904.
40. Ke Y, Li Z, Wu G, Zhang L, Tao M. A foldable underwater acoustic meta-structure with broadband sound absorption at low frequency. *Appl Phys Express*. 2022;15(6):067001.
41. Zhou X, Duan M, Xin F. Low-frequency underwater sound absorption of hybrid metamaterials using dissipative slow-sound. *Phys Lett A*. 2022;450:128361.
42. Wang Z, Huang Y, Zhang X, Li L, Chen M, Fang D. Broadband underwater sound absorbing structure with gradient cavity shaped polyurethane composite array supported by carbon fiber honeycomb. *J Sound Vib*. 2020;479:115375.
43. Ivansson SM. Numerical design of Alberich anechoic coatings with superellipsoidal cavities of mixed sizes. *J Acoust Soc Am*. 2008;124(4):1974-1984.
44. Qu S, Gao N, Tinel A, et al. Underwater metamaterial absorber with impedance-matched composite. *Sci Adv*. 2022;8(20):eabm4206.
45. Ashby MF, Brechet YJM. Designing hybrid materials. *Acta Mater*. 2003;51(19):5801-5821.
46. Ashby MF. Hybrids to fill holes in material property space. *Philos Mag*. 2005;85(26-27):3235-3257.
47. Yan LL, Yu B, Han B, Chen CQ, Zhang QC, Lu TJ. Compressive strength and energy absorption of sandwich panels with aluminum foam-filled corrugated cores. *Compos Sci Technol*. 2013;86:142-148.
48. Han B, Qin K, Yu B, Wang B, Zhang Q, Lu TJ. Honeycomb-corrugation hybrid as a novel sandwich core for significantly enhanced compressive performance. *Mater Des*. 2016;93:271-282.
49. Tang Y, Li F, Xin F, Lu TJ. Heterogeneously perforated honeycomb-corrugation hybrid sandwich panel as sound absorber. *Mater Des*. 2017;134:502-512.
50. Tang Y, Ren S, Meng H, et al. Hybrid acoustic metamaterial as super absorber for broadband low-frequency sound. *Sci Rep*. 2017;7:43340.
51. Tang Y, Xin F, Lu TJ. Sound absorption of micro-perforated sandwich panel with honeycomb-corrugation hybrid core at high temperatures. *Compos Struct*. 2019;226:111285.
52. Kanso MA, Giacomin AJ, Saengow C, Piette JH. Macromolecular architecture and complex viscosity. *Phys Fluids*. 2019;31(8):087107.
53. Zhao H, Liu Y, Yu D, Wang G, Wen J, Wen X. Absorptive properties of three-dimensional phononic crystal. *J Sound Vib*. 2007;303(1-2):185-194.
54. Yang H, Li Y, Zhao H, Wen J, Wen X. Acoustic anechoic layers with singly periodic array of scatterers: computational methods, absorption mechanisms, and optimal design. *Chin Phys B*. 2014;23(10):283-291.
55. COMSOL Multiphysics® v. 5.4. cn.comsol.com. COMSOL AB. Stockholm, Sweden.
56. Yu C, Duan M, He W, Xin F, Lu TJ. Underwater anechoic layer with parallel metallic plate insertions: theoretical modelling. *J Micromech Microeng*. 2021;31(7):074002.
57. Zhang Y, Pan J, Chen K, Zhong J. Subwavelength and quasi-perfect underwater sound absorber for multiple and broad frequency bands. *J Acoust Soc Am*. 2018;144(2):648-659.
58. Gao N, Lu K. An underwater metamaterial for broadband acoustic absorption at low frequency. *Appl Acoust*. 2020;169:107500.

AUTHOR BIOGRAPHIES

Chenlei Yu is a PhD student at School of Aerospace Engineering, Xi'an Jiaotong University, Xi'an, China. He received his bachelor's degree from the same university in 2018. Currently, he is working on underwater sound absorption and acoustic metamaterials.

Mingyu Duan is a PhD student at the Department of Advanced Manufacturing and Robotics, Peking University, Beijing, China. He received his master's degree from the School of Aerospace Engineering, Xi'an Jiaotong University, Xi'an, China, in 2021. Currently, he is working on acoustic metamaterials and soft matter physics.

Wei He is a PhD student at the School of Aerospace Engineering, Xi'an Jiaotong University, Xi'an, China. He received his bachelor's degree from the same university in 2016. His current focus is on the acoustic behaviors of regular porous materials.

Xin Chen is an engineer at Xi'an Modern Chemistry Research Institute, Xi'an, China. He received his PhD from the School of Aerospace Engineering (Xi'an Jiaotong University, Xi'an, China) in 2020. His current focus is on the mechanical behaviors of porous composites.

Fengxian Xin is a professor at the School of Aerospace Engineering of Xi'an Jiaotong University, Xi'an, China. He received his PhD from the same university. Currently, he is a visiting scholar at Harvard University and a visiting scholar at MIT. He is working on acoustic wave dynamics, mainly soft media multifield coupling mechanics, porous media vibration and noise reduction, multifunctional design of hydroacoustic materials, and so on.

Tian J. Lu is a professor at the School of Aeronautics and Astronautics of Nanjing University of Aeronautics and Astronautics, Nanjing, China. He is the founding director of the MOE Key Laboratory for Multifunctional Materials and Structures (LMMS) and the MIIT Key Laboratory of Multifunctional Lightweight Materials and Structures (MLMS). He was lecturer, reader, and professor of materials engineering at the Cambridge University Engineering Department from 1996 to 2006. During this period, he was also a fellow and director of studies of Queens' College, Cambridge University. Between 2005 and 2016, he was the chief scientist for the National Basic Research Program (973 Project) of China. He is the recipient of many prestigious awards, including the National Natural Science Award of China and the Young Chinese Scientist Award. He is the editor-in-chief of *Acta Mechanica Sinica* (AMS), the founding editor of the *International Journal of Applied Mechanics*, and also serves as the associate editor or member of the editorial board for more than 10 professional journals. From 2010 to 2014, he served as the vice president of the Chinese Society of Theoretical and Applied Mechanics (CSTAM). At present, representing China, he holds important positions in the International Union of Theoretical and Applied Mechanics (IUTAM). He is a fellow of American Institute for Medical and Biological Engineering (AIMBE). He uses theoretical, experimental, and numerical approaches to investigate key research frontiers in engineering sciences, addressing challenges in the mechanics of materials, noise and vibration, heat transfer, and biomechanics.

How to cite this article: Yu C, Duan M, He W, Chen X, Xin F, Lu TJ. Grating-like anechoic layer for broadband underwater sound absorption. *Int J Mech Syst Dyn*. 2022;1-13. doi:10.1002/msd2.12053